Noise Removed Inconsistency Activation Map for Unsupervised Registration of Brain Tumor MRI between Pre-operative and Follow-up Phases

Chongwei Wu[1†], Xiaoyu Zeng[1†], Hao Wang[1], Xu Zhang[2], Wei Fang[2], Qiang Li[1(✉)], and Zhiwei Wang[1(✉)]

[1] Wuhan National Laboratory for Optoelectronics, Huazhong University of Science and Technology, Wuhan, China
[2] Wuhan United Imaging Healthcare Surgical Technology Co., Ltd, Wuhan, China

Abstract. Structure inconsistency is the key challenge in registration of brain MRI between pre-operative and follow-up phases, which misguides the objective of image similarity maximization, and thus degrades the performance significantly. The current solutions rely on bidirectional registration to find the mismatched deformation fields as the inconsistent areas, and use them to filter out the unreliable similarity measurements. However, this is sensitive to the accumulated registration errors, and thus yields inaccurate inconsistent areas. In this paper, we provide a more efficient and accurate way, by letting the registration model itself to 'speak out' a Noise Removed Inconsistency Activation Map (NR-IAM) as the indicator of structure inconsistencies. We first obtain an IAM by use of the gradient-weighted feature maps but adopting an inverse direction. With this manner only, the resulting inconsistency map often occurs false highlights near some common structures like venous sinus. Therefore, we further introduce a statistical approach to remove the common erroneous activations in IAM to obtain NR-IAM. The experimental results on both public and private datasets demonstrate that by use of our proposed NR-IAM to guide the optimization, the registration performance can be significantly boosted, and is superior over that relying on the bidirectional registration by decreasing mean registration error by 5% and 4% in near tumor and far from tumor regions, respectively. Codes are available at https://github.com/chongweiwu/NR-IAM.

Keywords: Structural Inconsistency · Inconsistency Activation Map · Unsupervised Registration.

1 Introduction

Accurate registration of longitudinal brain MRI between pre-operative and follow-up phases is crucial to treatment decision, therapy assessment and signatures analysis for infiltrated tissues [1,15]. However, there are various challenges,

[†] Equal contribution.

and among them structural inconsistency across images, caused by tumor's resection and recurrence, is the key issue that prevents high-quality performance [3].

Forcibly maximizing the similarity of images containing inconsistencies like [18, 25] leads to chaotic deformations of those inconsistent areas, and also negatively affects the surrounding normal tissue registration. Various approaches have been proposed to combat this problem, and can mainly divide into: *1) Reconstruction-based method* [10, 11, 16, 17] and *2) Mask-based method* [5,7,9,14,20]. Reconstruction-based methods convert abnormal images to pseudo-normal images, and introduce the pseudo appearance to guide the spatial transformation of lesions. However, modeling pseudo appearance with statistical models [11,16] require additional data from healthy populations. Some inpainting methods [10,24] learn from the normal regions of abnormal images, requiring extra segmentation of lesions. Moreover, these reconstruction models learning from normal tissues cannot simulate the pseudo-normal appearance with mass effect, leaving the incosistency issue still unsolved.

Mask-based methods remove the similarity measurement of inconsistency to avoid the implausible deformations. However, these methods require accurate localization of inconsistent regions. Earlier studies [5, 7] rely on manual delineations, which are labor-intensive and costly. Alternatively, some unsupervised schemes [6, 20, 21] have been proposed. Risholm *et al.* [21] detects the inconsistencies by a level set method evolving in the space where image intensities disagree. Liu *et al.* [17] applies a seg-model based on minimal mutual information to distinguishes inconsistency areas from background. However, their location is independent of the registration task, which may restrict the performance of registration. Then, Mok *et al.* [20] leverages a forward-backward consistency of deformation fields to find the mismatch as inconsistencies. However, it yields inaccurate inconsistency areas with the disturb of accumulated registration errors.

Therefore, to effectively address the inconsistency issue in abnormal image registration, locating registration-target-specific inconsistency is necessary. In this paper, we present a novel mask-based method, by visualizing the deep representation of registration model to obtain a Noise Removed Inconsistency Activation Map (NR-IAM), for robust localization and registration of inconsistent areas in a coupled way. Our motivation is based on the Class Activation Mapping techniques [23, 26], which can creatively locate target-specific regions via weighted feature maps. To this end, we have inconsistency activation map (IAM) acquired from the reverse activation of feature maps. However, the resulting map contains noise activations near some common structures like venous sinus. Thanks to the homogeneity of brain tissue and structure, we thus propagate global activations into a target space and subsequently superimpose the global maps to extract the common erroneous activations, which are finally removed from the IAM to obtain NR-IAM. In summary, our key contributions include:

- We propose a novel NR-IAM, firstly introducing target-specific inconsistency map for unsupervised registration of brain tumor MRI.
- We propose a reverse activated IAM that reveals the target-specific inconsistencies. Then, permitted by the homogeneity of brain tissue, we obtain a

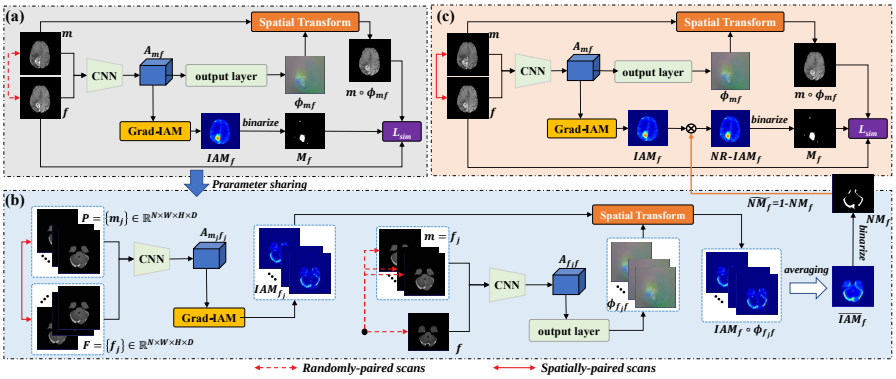

Fig. 1. Diagram of our proposed framework. (a) Pretraning with IAM, (b) Extraction of common erroneous activations and (c) Finetuning with NR-IAM.

superimposed noise map to remove the common erroneous activations of the inconsistency map.

– Extensive and comprehensive experimental results on both public and private datasets demonstrate that NR-IAM outperforms the state-of-the-arts (SOTA) by decreasing the mean target registration error at least by 4% and shows the superior localization abilities for inconsistency.

2 Methods

As shown in Fig. 1, to better register abnormal images, we introduce Gradient-Weighted Inconsistency Activation Mapping (Grad-IAM) layer to perceive target-specific inconsistencies and Noise Mapping Process (NMP) to statistic the common erroneous activations. Thus, NR-IAM acquired from the collaborations of the two modules can effectively locate inconsistencies. We will detail how to obtain IAM, common erroneous activations and implement model training.

2.1 IAM Acquired from Grad-IAM

Inspired by Grad-CAM [23], we propose Grad-IAM to locate the inconsistencies across the registered moving $m \circ \phi_{mf}$ and fixed f images, where ϕ_{mf} and "$\circ$" indicate displacement field and spatial transformation, respectively.

We build our method on top of 3-level clapIRN [19] and extend it for unsupervised location and registration of scans with structural inconsistency. Our model takes m and f as inputs and produces a combined displacement field ϕ_{mf} and intermediate feature maps $A_{mf} \in \mathbb{R}^{C \times W \times H \times D}$, generated by the penultimate convolution layer, as outputs. Then, we back propagate the gradient of images similarity to the c-th feature map A^c_{mf}, obtaining the corresponding weight w^c_{mf}:

$$w^c_{mf} = \frac{1}{Z} \sum_{x \in \Omega} \frac{\partial Sim(f, m \circ \phi_{mf})}{\partial A^c_{mf}(x)}. \tag{1}$$

where $Sim(\cdot)$, x and Z indicate the similarity measure, voxel space over 3-dimensional space Ω and voxel number, respectively. Then, we reverse the weight and compute channel-wise inconsistencies to obtain inconsistency map IAM_f:

$$IAM_f = \sum_{c \in C} ReLU(-w_{mf}^c \times A_{mf}^c). \tag{2}$$

2.2 Common Erroneous Activations Extracted from NMP

The IAM acquired from Grad-IAM contains erroneous activations, near some common structures like venous sinus. Fortunately, brain tissue and structure exhibit homogeneity, while tumor's occurrences are dispersed. Therefore, a global superimposed IAM may aid to the localization of the common noises. We thus propose NMP in Fig. 1(b) to extract the common erroneous activations.

Let $P = \{m_j\} \in \mathbb{R}^{N \times W \times H \times D}$ and $F = \{f_j\} \in \mathbb{R}^{N \times W \times H \times D}$ be the pre-operative and follow-up datasets in the training set, respectively. Firstly, we employ a pretrained model in Fig. 1(a) to exploit global activation information. Each spatially-paired scans, m_j and f_j, are fed into the pretrained model to obtain coarse activation map IAM_{f_j}. Then, we reuse the pretrained model to estimate displacement fields $\phi_{f_j f}$, propagating each corresponding activation map IAM_{f_j} into a target space of f. Now, a spatial average pooling retains the common erroneous activations $\overline{IAM}_f$:

$$\overline{IAM}_f = \frac{1}{N} \sum_{j \in N} IAM_{f_j} \circ \phi_{f_j f}. \tag{3}$$

Moreover, a $1/0$ indicator is utilized to extract the noise mask NM_f:

$$NM_f = \begin{cases} 1, & if \quad \dfrac{\overline{IAM}_f - mean(\overline{IAM}_f)}{std(\overline{IAM}_f)} \geq \beta \\ 0, & else. \end{cases} \tag{4}$$

where β is a threshold manually set as 2.6. Then $\widetilde{NM}_f = 1 - NM_f$ is multiplied with IAM_f (acquired from fine-tuning model) to obtain a noise removed inconsistency map $NR\text{-}IAM_f$.

2.3 Model Training

In the pretraining stage (Fig. 1(a)), we randomly select m and f from P and F as training pair, and use the coarse inconsistency maps IAM_f and IAM_m for optimization, where the IAM_f and IAM_m are binarized with Eq. (4) to obtain M_f and M_m for the masking of inconsistency voxels. While in the later fine-tuning stage (Fig. 1(c)), we finetune the pretrained model with spatially-paired scans, m and f, and use the $NR\text{-}IAM_f$ and $NR\text{-}IAM_m$ for optimization, where the $NR\text{-}IAM_f$ and $NR\text{-}IAM_m$ are binarized with Eq. (4) to obtain M_f and M_m for the masking of inconsistency voxels.

Objective functions With the inconsistency masks M_f and M_m, we optimize our framework by using 3 loss functions: L_{sim}, L_{reg} and L_{bid}. L_{sim} is a similarity term to minimize the dissimilarity between m and f at consistent areas, which is formulated as:

$$L_{sim} = -NLCC(f, m \circ \phi_{mf}) \times \widetilde{M}_f - NLCC(m, f \circ \phi_{fm}) \times \widetilde{M}_m. \quad (5)$$

where NLCC indicate normalized local cross-correlation. ϕ_{mf} and ϕ_{fm} represent forward and backward displacement fields, respectively. L_{reg} is a regular term to penalize implausible deformation and regularize contiguous motion to propagate deformation from correspondence surroundings to non-correspondence parts, which can be formulated as:

$$L_{reg} = \|\phi_{mf}\|_2^2 + \|\phi_{fm}\|_2^2. \quad (6)$$

L_{bid} is a bidirectional constraint to penalize the invertible transforms at correspondence regions. Mathematically, L_{bid} is calculated as:

$$L_{bid} = \sum \delta_{mf} \times \widetilde{M}_f + \delta_{fm} \times \widetilde{M}_m. \quad (7)$$

both $\delta_{mf}(x) = |\phi_{mf}(x) + \phi_{fm}(x + \phi_{mf}(x))|_2$ and $\delta_{fm}(x) = |\phi_{fm}(x) + \phi_{mf}(x + \phi_{fm}(x))|_2$ represent the symmetrical error of bidirectional transforms. Finally, the complete training loss can be written as:

$$L_{total} = L_{sim} + L_{reg} + L_{bid}. \quad (8)$$

3 Experiments

3.1 Datasets and Implementation Details

Dataset and Preprocess We evaluate NR-IAM on a public dataset, i.e., BraTS-Reg [3] and a private dataset. **BraTS-Reg** is a multimodal dataset that contains 160 pairs of pre-operative and follow-up brain tumor MRI scans. Among them, 140 pairs are annotated with 6 to 50 matching landmarks in both scans. We follow [20] to conduct 5-fold cross-validation on contrast-enhanced T1-weighted (T1ce) scans of the 140 cases. The **Private** dataset contains 254 unpaired T1ce scans, of which 109 are labeled with tumors by experienced clinicians, while the remaining 146 scans are not. We combine the unlabeled images and BraTS-Reg as training data, and use the labeled data for validation. Specifically, we align an almost normal scan to the others for validation.

To ensure the approaches focused on the deformable registration problem, all included scans are reoriented to the RAS orientation with a 1 mm^3 isotropic resolution and affinely aligned to the anatomical template (i.e., SRI24 atlas [22]). Then, to reasonably evaluate registration performance, we divide brain tumor images into 4 separate regions, i.e, tumor, near tumor (within 30 mm of tumor boundary), far from tumor (over 30 mm of tumor boundary) and background regions. We only measure the registration performance in near tumor (region 1) and far from tumor (region 2) regions. For BraTS-Reg, we use the DeepMedic [12] to obtain tumor segmentation of each pre-operative scan to divide the 4 regions. For private data, we use the labeled tumor to distinguish the 4 regions.

Table 1. Comparison results of various methods on BraTS-Reg dataset. The best is marked in bold. initial: spatial normalization. ↑: higher is better, and ↓: lower is better.

Method	Near Tumor			Far from tumor		
	TRE ↓	Robustness ↑	$\lvert J_\phi\rvert \leq 0(\%)$ ↓	TRE ↓	Robustness ↑	$\lvert J_\phi\rvert \leq 0(\%)$ ↓
initial	6.95 ± (5.21)	-	-	5.64 ± (5.08)	-	-
Elastix	3.62 ± (2.67)	0.80 ± (1.92)	**0.00** ± (0.00)	2.16 ± (1.92)	0.77 ± (0.27)	**0.00** ± (0.00)
Ants	4.87 ± (5.69)	0.56 ± (0.35)	**0.00** ± (0.00)	2.74 ± (0.28)	0.54 ± (0.27)	**0.00** ± (0.00)
VoxelMorph	3.85 ± (2.69)	0.79 ± (0.30)	0.16 ± (0.83)	2.08 ± (0.94)	0.81 ± (0.24)	0.14 ± (0.15)
VoxelMorph-diff	3.92 ± (2.75)	0.79 ± (0.29)	**0.00** ± (0.00)	2.09 ± (1.02)	0.77 ± (0.27)	**0.00** ± (0.00)
cLapIRN	3.73 ± (2.83)	0.77 ± (0.29)	0.35 ± (0.76)	1.96 ± (1.07)	0.81 ± (0.25)	0.21 ± (0.31)
DIRAC	3.36 ± (2.47)	0.80 ± (0.29)	0.48 ± (0.76)	1.85 ± (0.85)	0.81 ± (0.24)	0.17 ± (0.27)
NR-IAM	**3.18** ± (2.45)	**0.81** ± (0.29)	0.02 ± (0.05)	**1.77** ± (0.80)	**0.82** ± (0.24)	0.02 ± (0.08)

Table 2. Comparison results of various methods on private dataset.

Method	Near Tumor			Far from tumor		
	NCC ↑	MI ↑	$\lvert J_\phi\rvert \leq 0(\%)$ ↓	NCC ↑	MI ↑	$\lvert J_\phi\rvert \leq 0(\%)$ ↓
Elastix	0.593 ± (0.116)	0.533 ± (0.141)	**0.00** ± (0.00)	0.648 ± (0.041)	0.606 ± (0.041)	**0.00** ± (0.00)
Ants	0.640 ± (0.122)	0.557 ± (0.160)	**0.00** ± (0.00)	0.718 ± (0.053)	0.689 ± (0.087)	**0.00** ± (0.00)
VoxelMorph	0.645 ± (0.107)	0.582 ± (0.147)	0.15 ± (0.23)	0.691 ± (0.040)	0.673 ± (0.078)	0.10 ± (0.11)
VoxelMorph-diff	0.652 ± (0.104)	0.581 ± (0.146)	**0.00** ± (0.00)	0.697 ± ((0.039)	0.669 ± (0.077)	**0.00** ± (0.00)
cLapIRN	0.820 ± (0.061)	0.838 ± (0.197)	3.22 ± (1.63)	0.874 ± (0.021)	0.955 ± (0.099)	1.70 ± (0.44)
DIRAC	0.826 ± (0.060)	0.853 ± (0.204)	1.33 ± (0.52)	0.877 ± (0.021)	0.996 ± (0.101)	0.81 ± ((0.19)
NR-IAM	**0.831** ± (0.058)	**0.883** ± (0.200)	0.60 ± (0.55)	**0.882** ± (0.019)	**1.015** ± (0.102)	0.21 ± (0.16)

Implementation Details For learning-based methods, we resize input scans to 160×160×80, set the batch size to 1 and use Adam optimizer with a fixed learning rate 1e-4 for optimization. Then, we upsample the output displacement fields to 1 mm^3 isotropic resolution with bi-linear interpolation for evaluation. We implement all these methods with PyTorch 1.10 on a platform containing a GPU resource of NVIDIA RTX 4090 and a CPU resource of Intel Xeon Gold 6230R.

Measurements Five measurements are considered in this study, where two (the average target registration error (TRE) and robustness) measure the point-wise similarity, two (NCC and MI) measure the image-wise similarity, and one, i.e., the percentage of the number of values in the Jacobian determinant that are no greater than 0 (denote as $|J_\phi| \leq 0(\%)$) measures the local invertibility of deformation. We follow [20] to register each pre-operative scan to follow-up scan and invert the landmarks of follow-up scan to the corresponding landmarks of pre-operative scan to measure the TRE with Euclidean distance in millimetres, and define the robustness as the proportion of successfully registered landmarks in each case. We calculate NCC, MI and $|J_\phi| \leq 0(\%)$ in the foreground regions.

3.2 Results and Discussions

Comparison with other methods We compare NR-IAM with two conventional methods, i.e., Elastix [13] and ANTs [2], and four learning-based networks, i.e., VoxelMorph [4], VoxelMorph-diff [8] cLapIRN and DIRAC [20] (an open-sourced SOTA method) on both public and private datasets. Table 1 gives the

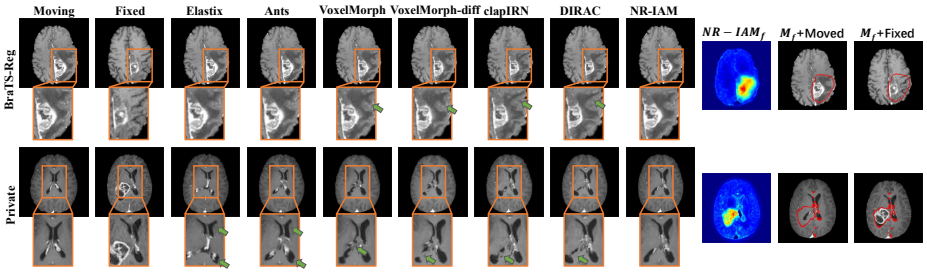

Fig. 2. Visualization of warped results (P to F) from different registration methods. Implausible deformations are highlighted with green arrows. The estimated inconsistent maps and regions of our method are shown next to our results, where the regions are overlaid with both moved and fixed images (in red).

comprehensive results of various methods in regions 1 and 2 across the 140 subjects of BraTS-Reg. Comparing to other methods, the lower average TRE, higher robustness and second best $|J_\phi| \leq 0(\%)$ of NR-IAM in both regions indicate our method achieves the best overall performance. Specially, NR-IAM has the lowest average TRE of 3.18 and 1.77 mm in region 1 and 2, respectively, which reduces average TRE by 0.18 mm (5%) and 0.08 mm (4%) compared to DIRAC.

We also conduct experiments on our private dataset. Table 2 gives the quantitative results in the 2 regions. As can be seen, our method achieves the best performance compared to other methods in terms of all metrics except the $|J_\phi| \leq 0(\%)$. Meanwhile, Fig. 2 visualize the registration results of each method and the estimated inconsistency maps and inconsistent regions of NR-IAM on the two datasets. The results present that our method can accurately locating inconsistencies, i.e, tumor and edema regions across the registered images, and can better reduce implausible deformations in the patients-specific image registration compared to other methods.

Comparison with different masks We further report the results of baseline method clapIRN optimized with 6 masks on BraTS-Reg for comparison, where two trained with tumor core and whole tumor acquired from DeepMedic, one trained with mask inferred by NLCC Loss, and three trained with learning-based masks acquired from inversely operated Grad-CAM (denoted as Grad-CAM$^-$), DIRAC and NR-IAM, respectively. Table 3 shows that NR-IAM achieves the best performance in terms of all metrics except the robustness term in region 2. Notably, NR-IAM overally decreases the average TRE of other masks by 0.23 mm (7%) and 0.10 mm (5%) in regions 1 and 2, respectively. And the localization results in Fig. 3 indicate our method can more accurately locate stuctural inconsistencies across registered scans compared to location acquired from NLCC Loss, Grad-CAM$^-$ and DIRAC.

Table 3. The results of cLapIRN optimized with various masks on BraTS-Reg dataset.

Method	Near Tumor		Far from tumor	
	TRE ↓	Robustness ↑ $\lvert J_\phi\rvert < 0(\%)$ ↓	TRE ↓	Robustness ↑ $\lvert J_\phi\rvert < 0(\%)$ ↓

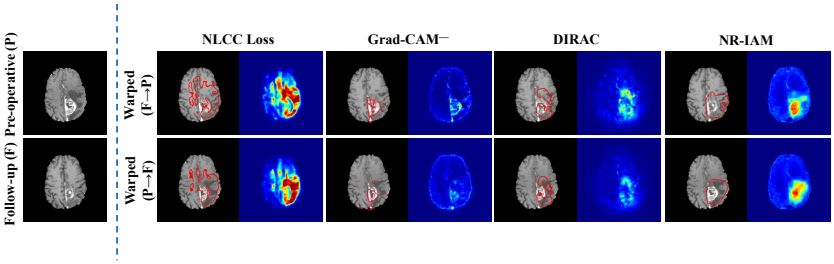

Fig. 3. Bidirectional location results from 4 unsupervised location methods. The estimated inconsistent regions are overlaid with warped images (in red). The inconsistency maps are shown next to the regions.

Ablation study We conduct an ablation study on BraTS-Reg to verify the effectiveness of our modules, i.e., Grad-IAM and NMP. The first variant is trained without the two modules. The second variant trained with Grad-IAM. The last variant trained with the collaborations of Grad-IAM and NMP. Results in Table 4 demonstrate the two modules well boost the registration performance, and the Grad-IAM can significantly decrease mean TRE of the first variant by 0.53 (14%) and 0.16 (8%) mm in region 1 and 2 (see the $1st$ and $3rd$ rows). Comparing to the second variant, we also observe that NMP slightly reduces the registration error by 1% and 2% (see the $2nd$ and $3rd$ rows) in region 1 and 2, respectively.

Table 4. The ablation study for each part of NR-IAM. Grad-IAM: gradient-weighted inconsistency mapping. NMP: noise mapping process.

Grad-IAM	NMP	Near Tumor			Far from tumor		
		TRE ↓	Robustness ↑ $\lvert J_\phi\rvert \leq 0(\%)$ ↓		TRE ↓	Robustness ↑ $\lvert J_\phi\rvert \leq 0(\%)$ ↓	
–	–	$3.73 \pm (2.83)$	$0.77 \pm (0.29)$	$0.35 \pm (0.76)$	$1.96 \pm (1.07)$	$0.81 \pm (0.25)$	$0.21 \pm (0.31)$
✓	–	$3.20 \pm (2.38)$	$0.81 \pm (0.27)$	$0.09 \pm (0.19)$	$1.80 \pm (1.07)$	$0.83 \pm (0.22)$	$0.03 \pm (0.12)$
✓	✓	$3.18 \pm (2.45)$	$0.81 \pm (0.29)$	$0.02 \pm (0.05)$	$1.77 \pm (0.80)$	$0.82 \pm (0.24)$	$0.02 \pm (0.08)$

4 Conclusion

We have presented a novel unsupervised registration method for brain MRI registration between pre-operative and follow-up phases, which can efficiently

locate inconsistent regions by letting the registration model itself to 'speak out' a NR-IAM. Specifically, we have NR-IAM obtained from Grad-IAM and purified by NMP. Hence, our registration performance can be significantly boosted. We verify our method on both public and private datasets. Experimental results demonstrate our method surpasses the SOTA method that relying on the bidirectional constraint. An ablation study also verified the effectiveness of our proposed modules, i.e. Grad-IAM and NMP. In the future, we attempt to enhance the localization of inconsistencies to improve the registration performances.

Acknowledgments. This research was funded in part by National Key R&D Program of China (Grant No. 2022YFE0200600), National Natural Science Foundation of China (Grant No. 62202189), Fundamental Research Funds for the Central Universities (Grant No.2021XXJS033), and research grants from Wuhan United Imaging Healthcare Surgical Technology Co., Ltd.

Disclosure of Interests. The authors have no competing interests to declare that are relevant to the content of this article.

References

1. Akbari, H., Macyszyn, L., Da, X., Wolf, R.L., Bilello, M., Verma, R., O'Rourke, D.M., Davatzikos, C.: Pattern analysis of dynamic susceptibility contrast-enhanced mr imaging demonstrates peritumoral tissue heterogeneity. Radiology **273**(2), 502–510 (2014)
2. Avants, B.B., Tustison, N., Song, G., et al.: Advanced normalization tools (ants). Insight j **2**(365), 1–35 (2009)
3. Baheti, B., Waldmannstetter, D., Chakrabarty, S., Akbari, H., Bilello, M., Wiestler, B., Schwarting, J., Calabrese, E., Rudie, J., Abidi, S., et al.: The brain tumor sequence registration challenge: establishing correspondence between pre-operative and follow-up mri scans of diffuse glioma patients. arXiv preprint arXiv:2112.06979 (2021)
4. Balakrishnan, G., Zhao, A., Sabuncu, M.R., Guttag, J., Dalca, A.V.: Voxelmorph: a learning framework for deformable medical image registration. IEEE transactions on medical imaging **38**(8), 1788–1800 (2019)
5. Brett, M., Leff, A.P., Rorden, C., Ashburner, J.: Spatial normalization of brain images with focal lesions using cost function masking. Neuroimage **14**(2), 486–500 (2001)
6. Chitphakdithai, N., Duncan, J.S.: Non-rigid registration with missing correspondences in preoperative and postresection brain images. In: International Conference on Medical Image Computing and Computer-Assisted Intervention. pp. 367–374. Springer (2010)
7. Clatz, O., Delingette, H., Talos, I.F., Golby, A.J., Kikinis, R., Jolesz, F.A., Ayache, N., Warfield, S.K.: Robust nonrigid registration to capture brain shift from intraoperative mri. IEEE transactions on medical imaging **24**(11), 1417–1427 (2005)
8. Dalca, A.V., Balakrishnan, G., Guttag, J., Sabuncu, M.R.: Unsupervised learning of probabilistic diffeomorphic registration for images and surfaces. Medical image analysis **57**, 226–236 (2019)

9. Gooya, A., Pohl, K.M., Bilello, M., Cirillo, L., Biros, G., Melhem, E.R., Davatzikos, C.: Glistr: glioma image segmentation and registration. IEEE transactions on medical imaging **31**(10), 1941–1954 (2012)
10. Han, X., Shen, Z., Xu, Z., Bakas, S., Akbari, H., Bilello, M., Davatzikos, C., Niethammer, M.: A deep network for joint registration and reconstruction of images with pathologies. In: Machine Learning in Medical Imaging: 11th International Workshop, MLMI 2020, Held in Conjunction with MICCAI 2020, Lima, Peru, October 4, 2020, Proceedings 11. pp. 342–352. Springer (2020)
11. Han, X., Yang, X., Aylward, S., Kwitt, R., Niethammer, M.: Efficient registration of pathological images: a joint pca/image-reconstruction approach. In: 2017 IEEE 14th International Symposium on Biomedical Imaging (ISBI 2017). pp. 10–14. IEEE (2017)
12. Kamnitsas, K., Ledig, C., Newcombe, V.F., Simpson, J.P., Kane, A.D., Menon, D.K., Rueckert, D., Glocker, B.: Efficient multi-scale 3d cnn with fully connected crf for accurate brain lesion segmentation. Medical image analysis **36**, 61–78 (2017)
13. Klein, S., Staring, M., Murphy, K., Viergever, M.A., Pluim, J.P.: Elastix: a toolbox for intensity-based medical image registration. IEEE transactions on medical imaging **29**(1), 196–205 (2009)
14. Kwon, D., Niethammer, M., Akbari, H., Bilello, M., Davatzikos, C., Pohl, K.M.: Portr: pre-operative and post-recurrence brain tumor registration. IEEE transactions on medical imaging **33**(3), 651–667 (2013)
15. Kwon, D., Zeng, K., Bilello, M., Davatzikos, C.: Estimating patient specific templates for pre-operative and follow-up brain tumor registration. In: Medical Image Computing and Computer-Assisted Intervention–MICCAI 2015: 18th International Conference, Munich, Germany, October 5-9, 2015, Proceedings, Part II 18. pp. 222–229. Springer (2015)
16. Liu, X., Niethammer, M., Kwitt, R., Singh, N., McCormick, M., Aylward, S.: Low-rank atlas image analyses in the presence of pathologies. IEEE transactions on medical imaging **34**(12), 2583–2591 (2015)
17. Liu, Y., Gu, S.: Co-learning semantic-aware unsupervised segmentation for pathological image registration. In: International Conference on Medical Image Computing and Computer-Assisted Intervention. pp. 537–547. Springer (2023)
18. Meng, M., Bi, L., Feng, D., Kim, J.: Brain tumor sequence registration with non-iterative coarse-to-fine networks and dual deep supervision. In: International MICCAI Brainlesion Workshop. pp. 273–282. Springer (2022)
19. Mok, T.C., Chung, A.C.: Conditional deformable image registration with convolutional neural network. In: Medical Image Computing and Computer Assisted Intervention–MICCAI 2021: 24th International Conference, Strasbourg, France, September 27–October 1, 2021, Proceedings, Part IV 24. pp. 35–45. Springer (2021)
20. Mok, T.C., Chung, A.C.: Unsupervised deformable image registration with absent correspondences in pre-operative and post-recurrence brain tumor mri scans. In: International Conference on Medical Image Computing and Computer-Assisted Intervention. pp. 25–35. Springer (2022)
21. Risholm, P., Samset, E., Talos, I.F., Wells, W.: A non-rigid registration framework that accommodates resection and retraction. In: Information Processing in Medical Imaging: 21st International Conference, IPMI 2009, Williamsburg, VA, USA, July 5-10, 2009. Proceedings 21. pp. 447–458. Springer (2009)
22. Rohlfing, T., Zahr, N.M., Sullivan, E.V., Pfefferbaum, A.: The sri24 multichannel atlas of normal adult human brain structure. Human brain mapping **31**(5), 798–819 (2010)

23. Selvaraju, R.R., Cogswell, M., Das, A., Vedantam, R., Parikh, D., Batra, D.: Grad-cam: Visual explanations from deep networks via gradient-based localization. In: Proceedings of the IEEE international conference on computer vision. pp. 618–626 (2017)
24. Xing, F., Liu, X., Kuo, C.C.J., El Fakhri, G., Woo, J.: Brain mr atlas construction using symmetric deep neural inpainting. IEEE journal of biomedical and health informatics **26**(7), 3185–3196 (2022)
25. Zeineldin, R.A., Karar, M.E., Mathis-Ullrich, F., Burgert, O.: Self-supervised ireg-net for the registration of longitudinal brain mri of diffuse glioma patients. In: International MICCAI Brainlesion Workshop. pp. 25–34. Springer (2022)
26. Zhou, B., Khosla, A., Lapedriza, A., Oliva, A., Torralba, A.: Learning deep features for discriminative localization. In: Proceedings of the IEEE conference on computer vision and pattern recognition. pp. 2921–2929 (2016)